NANO LETTERS
Letter
Cite This: Nano Lett. 2018, 18, 6441−6448
pubs.acs.org/NanoLett

Water-Activated $VOPO_4$ for Magnesium Ion Batteries

Xiao Ji,[†,‡] Ji Chen,[†] Fei Wang,[†] Wei Sun,[†] Yunjun Ruan,[‡] Ling Miao,[‡] Jianjun Jiang,*[,‡] and Chunsheng Wang*[,†,§]

[†]Department of Chemical and Biomolecular Engineering, University of Maryland, College Park, Maryland 20742, United States
[‡]School of Optical and Electronic Information, Huazhong University of Science and Technology, 430074 Wuhan, Hubei, China
[§]Department of Chemistry and Biochemistry, University of Maryland, College Park, Maryland 20742, United States

Supporting Information

ABSTRACT: Rechargeable Mg batteries, using high capacity and dendrite-free Mg metal anodes, are promising energy storage devices for large scale smart grid due to low cost and high safety. However, the performance of Mg batteries is still plagued by the slow reaction kinetics of their cathode materials. Recent discoveries demonstrate that water in cathode can significantly enhance the Mg-ion diffusion in cathode by an unknown mechanism. Here, we propose the water-activated layered-structure $VOPO_4$ as a novel cathode material and examine the impact of water in electrode or organic electrolyte on the thermodynamics and kinetics of Mg-ion intercalation/deintercalation in cathodes. Electrochemical measurements verify that water in both $VOPO_4$ lattice and organic electrolyte can largely activate $VOPO_4$ cathode. Thermodynamic analysis demonstrates that the water in the electrolyte will equilibrate with the structural water in $VOPO_4$ lattice, and the water activity in the electrolyte alerts the mechanism and kinetics for electrochemical Mg-ion intercalation in $VOPO_4$. Theoretical calculations and experimental results demonstrate that water reduces both the solid-state diffusion barrier in the $VOPO_4$ electrode and the desolvation penalty at the interface. To achieve fast reaction kinetics, the water activity in the electrolyte should be larger than 10^{-2}. The proposed activation mechanism provides guidance for screening and designing novel chemistry for high performance multivalent-ion batteries.

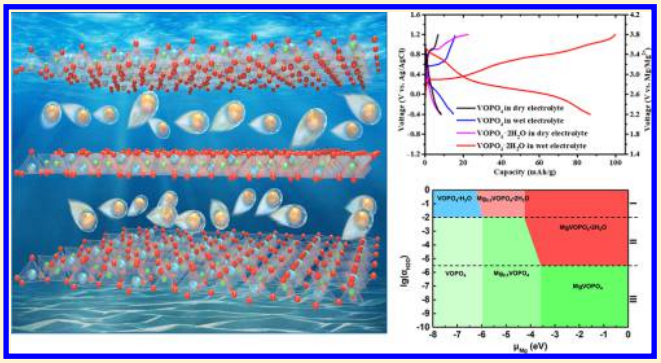

KEYWORDS: *Water cointercalation, layered $VOPO_4$, desolvation penalty, magnesium battery, first-principles calculation, water equilibrium*

The increasing demand of clean energy in modern society drives the search for reliable, sustainable electrochemical energy storage.[1] Among the various energy storage technologies, rechargeable lithium-ion batteries are currently the most attractive candidate.[2−4] However, increased concerns about the safety and cost of lithium-ion batteries are triggering the society to explore low cost and high energy "beyond Li-ion" technologies, such as Li−air,[5] Li−S,[6] sodium-ion,[7] and multivalent-ion (MV-ion) batteries.[8]

Among these "beyond Li-ion" technologies, the magnesium battery has drawn much attention due to high energy density, low cost, and high safety.[8,9] Although extensive efforts have been devoted to enhancing the performance of Mg-ion batteries,[10] only limited advance in performance of cathode materials has been achieved because of sluggish reaction kinetics or even deactivation of the host caused by the strong electrostatic interactions between Mg^{2+} ions and the anions in the host structure. Only few compounds, including Mo_6S_8,[10] V_2O_5,[11−13] MnO_2,[14−16] layered TiS_2,[17] $Li_xV_2(PO_4)_3$,[18] sulfur spinel compounds,[19,20] and Prussian blue analogues,[21,22] have been reported for Mg battery cathode materials. However, these cathodes either suffer from low energy density (such as Mo_6S_8, Prussian blue) or poor rate performance and cycle life (such as V_2O_5, MnO_2, layered TiS_2,[17] $Li_xV_2(PO_4)_3$).

Recently, it was reported that the introduction of H_2O into the organic electrolyte can significantly improve the electrochemical performance of the multivalent-ion cathodes,[23−25] and it is believed that the water in electrolytes can be inserted into cathode lattice by cointercalation of Mg with coordinated water molecules[26−28] and that the intercalated crystal water in MnO_2 can change the MnO_2 phase from spinel to a layered Birnessite structure,[29] enlarging the layered structure,[30] thus accelerating the MV-ion mobility. In addition, the strong-dipole water molecules presumably "shield" the charges of divalent Mg-ion and reduce the electrostatic interaction between the concentrated charges,[14,31,32] which also enhance the Mg-ion diffusivity. Theoretical calculation demonstrated that H_2O in wet electrolytes can shuttle with the Mg-ion

Received: July 12, 2018
Revised: August 13, 2018
Published: September 7, 2018

DOI: 10.1021/acs.nanolett.8b02854
Nano Lett. 2018, 18, 6441−6448

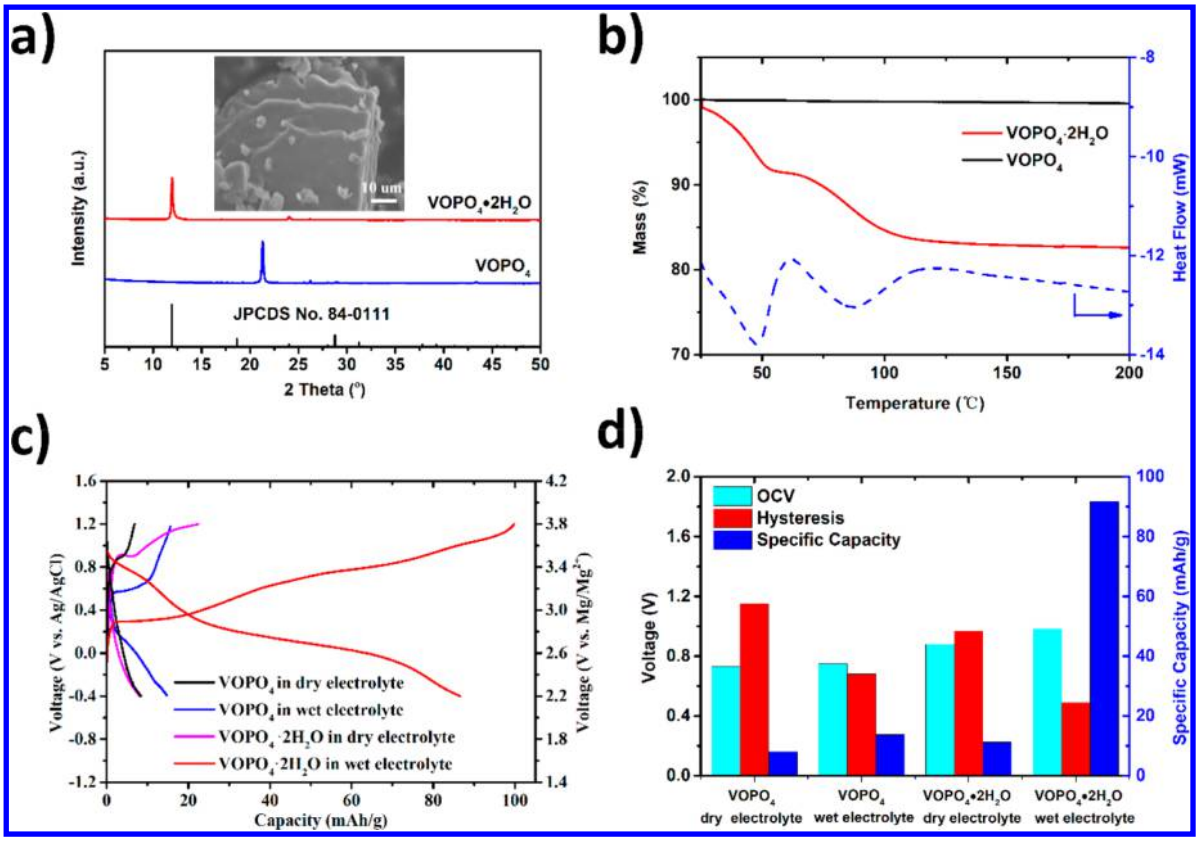

Figure 1. Material characterization and electrochemical performance of $VOPO_4$ cathode. (a) XRD pattern of layered $VOPO_4$ and $VOPO_4{\cdot}2H_2O$ cathode (inset: the SEM image of $VOPO_4{\cdot}2H_2O$). (b) Thermogravimetric analysis of $VOPO_4$ and $VOPO_4{\cdot}2H_2O$ powder measured between room temperature and 200 °C with a heating rate of 5 °C per min. (c) Typical voltage profiles of $VOPO_4$ and $VOPO_4{\cdot}2H_2O$ in dry (0.1 M $Mg(ClO_4)_2$-PC) and wet (0.1 M $Mg(ClO_4)_2{\cdot}6H_2O$-PC) electrolyte at a constant current density of 5 mA/g in a three-electrode cell with Ag/AgCl and active carbon as reference and counter electrode, respectively. The potential also converted to Mg/Mg^{2+} reference for convenience. (d) OCVs, hysteresis, and specific capacities of the tenth cycle for $VOPO_4$ and $VOPO_4{\cdot}2H_2O$ in dry and wet electrolytes. The hysteresis is calculated by subtracting the mid voltage of charge by that of discharge.

during Mg-ion insertion/extraction in Xerogel V_2O_5, yielding higher voltages and fast reaction rate.[33] Although the H_2O in the electrolyte and/or in the lattice of the layered structured host significantly changed the thermodynamics and kinetics of Mg-ion intercalation, the precise mechanism is still under debate. The systematic investigation of the role of water in the electrolyte and the host lattice will provide guidance for design of high-performance Mg-ion batteries.

In this work, we used layered $VOPO_4$ as a model cathode to systematically investigate the mechanism for water activation of an MV-ion cathode. The H_2O in the electrolyte exchanges and equilibrates with H_2O in $VOPO_4$ lattice, which alert the $VOPO_4$ structure and reaction pathway. The thermodynamic phase diagrams of $Mg{-}VOPO_4{-}H_2O$ at different Mg and H_2O contents were calculated. The solid-state diffusion barrier for Mg^{2+} intercalation into $VOPO_4{\cdot}nH_2O$ electrode and the desolvation energy penalty at the electrode−electrolyte interface were also investigated to provide insight into the kinetics for Mg-ion insertion/extraction in $VOPO_4{\cdot}nH_2O$ cathodes. The electrochemical performance of the anhydrous $VOPO_4$ and $VOPO_4{\cdot}2H_2O$ in the organic electrolytes with different H_2O content verified the theoretical calculation, revealing the mechanism for water activation of $VOPO_4$. The theoretical analysis on thermodynamics and kinetics of $VOPO_4{\cdot}nH_2O$ cathodes sheds light on the electrochemical performance of $VOPO_4{\cdot}nH_2O$ under different electrolytic conditions at an atomic scale.

Results and Discussion. The layered $VOPO_4{\cdot}2H_2O$ was synthesized using a hydrothermal method, and H_2O-free $VOPO_4$ was obtained by further dehydration of synthesized $VOPO_4{\cdot}2H_2O$ (Materials Synthesis, Supporting Information). Figure 1a demonstrates the X-ray diffraction (XRD) patterns of the layered $VOPO_4$ and $VOPO_4{\cdot}2H_2O$. All the peaks of $VOPO_4{\cdot}2H_2O$ and $VOPO_4$ can be indexed to tetragonal $VOPO_4{\cdot}2H_2O$ (JCPDS No. 84−0111) and $VOPO_4$ (JCPDS No. 27−0947), which belong to the *P*4/*nmm* space group. The peak of (001) plane of $VOPO_4{\cdot}2H_2O$ is located at $2\theta = 11.93°$, indicating an interlayer distance of d = 7.41 Å, which is significantly larger than that of anhydrous $VOPO_4$ (d = 4.17 Å). Therefore, the intercalation of water into $VOPO_4$ can be readily viewed using XRD. The scanning electron microscopy (SEM) image (inset of Figure 1a) shows the layered architecture of $VOPO_4{\cdot}2H_2O$. Furthermore, the content of H_2O in $VOPO_4{\cdot}2H_2O$ was determined from thermogravimetric analysis (TGA). From Figure 1b, the weight loss for $VOPO_4$ can be neglected, while that of $VOPO_4{\cdot}2H_2O$ is about 17.5%, corresponding to 1.91 H_2O per formula.

The electrochemical performances of the $VOPO_4{\cdot}2H_2O$ and $VOPO_4$ cathode were measured in a three-electrode cell using 0.1 M $Mg(ClO_4)_2$ or $Mg(ClO_4)_2{\cdot}6H_2O$ in propylene carbonate (PC) as electrolytes. Figure 1c demonstrates the first charge/discharge voltage profiles of $VOPO_4$ and $VOPO_4{\cdot}2H_2O$ in dry (0.1 M $Mg(ClO_4)_2$-PC) and wet (0.1 M $Mg(ClO_4)_2{\cdot}6H_2O$-PC) electrolyte, and the detailed capacities,

DOI: 10.1021/acs.nanolett.8b02854
Nano Lett. 2018, 18, 6441−6448

open circuit voltage (OCV), and voltage hysteresis are listed in Table 1. Only negligible capacity can be accessed from $VOPO_4$ in the dry electrolyte (8.0 mAh/g). $VOPO_4{\cdot}2H_2O$ in the wet electrolyte provides maximum capacity of 89 mAh/g in the first cycle, which is comparable to that of layered $V_2O_5{\cdot}nH_2O$.[34] However, just introducing water to either a $VOPO_4$ electrode or a $Mg(ClO_4)_2$-PC electrolyte could improve the capacity only slightly. The introduced water in electrode or electrolyte renders the increased capacity of $VOPO_4$, confirming that water can activate the $VOPO_4$ cathodes.

Table 1. Capacities (mAh/g), Hysteresis (V), and OCVs (V) for the Four Scenarios of $VOPO_4$ and $VOPO_4{\cdot}2H_2O$ in Wet and Dry Electrolytes

electrode	electrolyte	capacity	hysteresis	OCV
$VOPO_4$	$Mg(ClO_4)_2$-PC	8.0	1.15	0.73
$VOPO_4{\cdot}2H_2O$	$Mg(ClO_4)_2$-PC	11.2	0.97	0.88
$VOPO_4$	$Mg(ClO_4)_2{\cdot}6H_2O$-PC	13.8	0.68	0.75
$VOPO_4{\cdot}2H_2O$	$Mg(ClO_4)_2{\cdot}6H_2O$-PC	91.7	0.49	0.98

The OCVs, voltage hysteresis, and specific capacity of $VOPO_4$ after ten cycles with and without water in the electrode or electrolyte are summarized in Figure 1d. Thermodynamically, the OCVs are increased due to the presence of water in electrode and/or electrolyte, and the $VOPO_4{\cdot}2H_2O$ in the wet electrolyte exhibits the highest OCV. Kinetically, the voltage hysteresis was obtained by subtracting the mid voltage of charge from that of discharge to reflect the kinetics of the electrochemical process. Introducing water in both $VOPO_4$ electrode and electrolyte significantly reduces the voltage hysteresis from 1.15 to 0.49 V, indicating the obvious promotion of the kinetics. These results manifest that the presence of water has remarkable influence on the thermodynamics and kinetics of the electrochemical process.

Figure 1c shows that the water in either $VOPO_4$ interlayer or electrolyte increase the capacity, but $VOPO_4{\cdot}2H_2O$ in wet electrolyte has the highest capacity, also suggesting that H_2O exchange between interlayer of $VOPO_4$ and in the electrolyte. The exchange of H_2O in $VOPO_4$ and electrolyte during charge/discharge was characterized using XRD since the (001) peak position in XRD is highly sensitive to the H_2O and Mg^{2+} in a $VOPO_4$ lattice. As shown in Figure 2a, the right shift of the (001) peak after discharge indicates that the intercalation of Mg^{2+} ions into $VOPO_4{\cdot}2H_2O$ in a wet electrolyte reduces the interlayer distance. Upon charging, the (001) peak moves back but remains slightly right shifted compared to that of the original $VOPO_4{\cdot}2H_2O$ even the Mg-ion has been completely removed from $Mg_xVOPO_4{\cdot}2H_2O$ after holding at 1.2 V for 10 h before XRD characterization. This irreversible right shift in the (001) peak after complete Mg extraction from $Mg_xVOPO_4{\cdot}2H_2O$ is attributed to loss of H_2O from $Mg_xVOPO_4{\cdot}2H_2O$ since the H_2O in lattice of $VOPO_4$ tend to move into electrolyte to equilibrate with the H_2O in the wet electrolyte. A more severely positive shift in the (001) peak of $VOPO_4{\cdot}2H_2O$ after Mg-ion insertion and Mg-ion extraction in dry electrolyte further confirms the H_2O transport from $VOPO_4{\cdot}2H_2O$ into electrolytes (Figure 2a).

To fully understand the effect of H_2O on the thermodynamics of Mg^{2+} insertion into $VOPO_4$, DFT calculations at an atomic scale were performed. The $VOPO_4{\cdot}nH_2O$ with different water content (Figure S1, Supporting Information) was used to calculate the relative formation energy of each $Mg_xVOPO_4{\cdot}nH_2O$ with respect to phase separation between $VOPO_4$ and $MgVOPO_4$ structures when water activity is 1 ($\alpha = 1$) in wet electrolytes (Figure 2b). Green, blue, and red lines represent the stoichiometric coefficient n as 0, 1, and 2, respectively. The black dot−dash line indicates the energies of the global equilibrium ground states configuration of $Mg_xVOPO_4{\cdot}nH_2O$ phases. The result suggests that the equilibrium ground states of $Mg_xVOPO_4{\cdot}nH_2O$ are at a fully demagnesiated and half hydrated state ($x = 0$, $n = 1$), a half magnesiated and fully hydrated state ($x = 0.5$, $n = 2$), and a fully magnesiated and fully hydrated state ($x = 1$, $n = 2$) $VOPO_4$. The ground phase diagram indicates the electrochemical process can be illustrated as $VOPO_4{\cdot}H_2O \rightarrow Mg_{0.5}VOPO_4{\cdot}2H_2O \rightarrow MgVOPO_4{\cdot}2H_2O$ (Process I) in a wet electrolyte. Water cointercalates with Mg until $x_{Mg} = 0.5$ but then remains unchanged as more Mg-ions are inserted. The cointercalation of water with MV-ions has also been found in the $VOPO_4$ and V_2O_5 for zinc-ion batteries.[35,36] The relative energy difference among $VOPO_4{\cdot}nH_2O$ ($n = 0$, 1, and 2) is small, indicating the stability of these three phases are close in wet electrolyte.

More generally, the stability of all $Mg_xVOPO_4{\cdot}nH_2O$ phases were further evaluated as a function of α_{H2O} and Mg chemical potential (μ_{Mg}) by minimizing the grand-potential, as shown in Figure 2c. In this phase diagram, a high μ_{Mg} refers to highly magnesiated while decreasing the μ_{Mg} corresponds to the demagnesiation process. The increase in α_{H2O} represents more water in the electrolyte, and a water activity of 10^{-4} corresponds to ∼10 ppm by weight of water under the ideal solution approximation in solvents.[33] Each colored region stands for the stable phase under the state of charge and electrolytic condition. The boundaries represent the coexistence of two phases, while the three-phase coexistence is marked with triple points. According to Figure 2c, when Mg intercalation occurs from an electrolyte with water activity above 10^{-2}, Process I works. For an electrolyte with water activity in the range between 10^{-5} to 10^{-2}, $VOPO_4 \rightarrow Mg_{0.5}VOPO_4 \rightarrow MgVOPO_4{\cdot}2H_2O$ (Process II) would be the electrochemical process. For an electrolyte with water activity below 10^{-5}, $VOPO_4 \rightarrow Mg_{0.5}VOPO_4 \rightarrow MgVOPO_4$ (Process III) would be the main reaction route.

Accordingly, the average equilibrium voltage of the electrochemical processes under different electrolytic conditions were evaluated, as illustrated in Figure 2d. The red curve indicates the high-voltage two-phase transformation plateau ($0 \leq x \leq 0.5$), and the blue curve represents the low-voltage two-phase transformation plateau ($0.5 \leq x \leq 1$). The plateaus also correspond to the redox couple of V^{5+}/V^{4+} and V^{4+}/V^{3+}, respectively. The slopes indicate the intercalation voltage change, while Mg and H_2O cointercalation takes place. The V^{5+}/V^{4+} voltage plateau decreases as water activity decreases from 3.10 to 2.95 V as the water activity decreases from 1 to 10^{-2} and then maintain the voltage. The V^{4+}/V^{3+} voltage plateau stays at 2.19 V until the water activity becomes lower than 10^{-2}. In the range of water activity from 10^{-2} to 10^{-5}, H_2O exits from the structure with Mg-ions, decreasing the voltage to 1.79 V. It is apparent that the voltage increases with the increase of the water activity. This increase can be explained by realizing higher activity of water in electrolyte can supply more water to the electrode, which can stabilize the Mg_xVOPO_4 structures. However, it should be noted that adding water to the electrolyte narrows the electrolytic potential window. At a low water concentration in the electrolyte, the low voltage plateau of $Mg_xVOPO_4{\cdot}nH_2O$ is

DOI: 10.1021/acs.nanolett.8b02854
Nano Lett. 2018, 18, 6441−6448

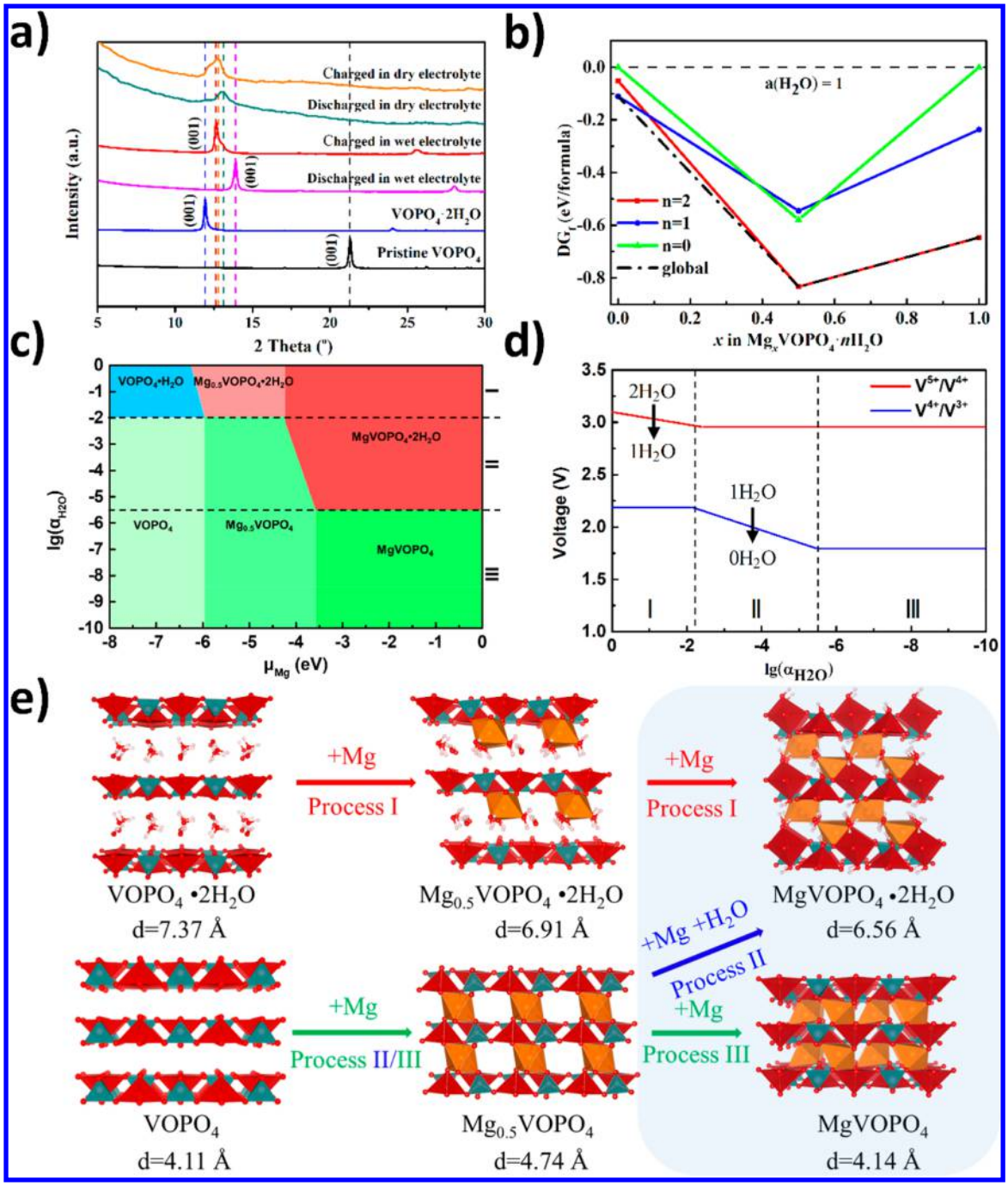

Figure 2. Thermodynamic investigation of $VOPO_4$ as Mg-ion battery cathode. (a) XRD patterns for pristine $VOPO_4$, $VOPO_4{\cdot}2H_2O$, and $VOPO_4{\cdot}2H_2O$ after charge and discharge in wet and dry electrolyte. (b) Relative formation energy per formula unit with respect to Mg concentration in electrolytic condition with water activity of 1. Green, blue, and red lines represent n = 0, 1, and 2 for $Mg_xVOPO_4{\cdot}nH_2O$, and the black dot−dash line stands for the global equilibrium ground state configuration. (c) Phase diagram of $Mg_xVOPO_4{\cdot}nH_2O$ as a function of water activity of electrolyte (α_{H_2O}) and Mg chemical potential (μ_{Mg}). The dash lines indicate the water activity range for different processes. (d) Calculated average equilibrium voltage (vs Mg/Mg^{2+}) for low and high Mg concentrations as a function of water activity of the electrolyte. The arrows indicate the exit of the water. (e) Illustration of typical electrochemical process under different electrolyte conditions. The interlayer distances are listed next to the corresponding structures. The light blue region indicating the equilibrium voltage is calculated to be lower than the water decomposition voltage.

lower than the water decomposition voltage; thus, only one electron can be stored per formula $VOPO_4{\cdot}2H_2O$, i.e., x = 0.5 Mg, reducing the capacity.

Therefore, the change in the XRD pattern after charge and discharge can be explained by the aforementioned analysis. The reduction in the interlayer distance in Figure 2a during Mg^{2+} ion intercalation into the interlayer of $VOPO_4{\cdot}2H_2O$ is attributed to the strong electrostatic interaction between Mg^{2+} ions and O atoms in water and on the $VOPO_4$ layer, which decreases the interlayer distance of $VOPO_4{\cdot}2H_2O$ (Figure 2e). Upon Mg-ion deintercalation (charging), water molecules in the $VOPO_4{\cdot}2H_2O$ exit with Mg^{2+} forming $VOPO_4{\cdot}nH_2O$ (n < 2), which makes the slight shift of (001) peak of $VOPO_4{\cdot}2H_2O$ (Figure 2a). The water content in $VOPO_4{\cdot}nH_2O$ also changes

DOI: 10.1021/acs.nanolett.8b02854
Nano Lett. 2018, 18, 6441−6448

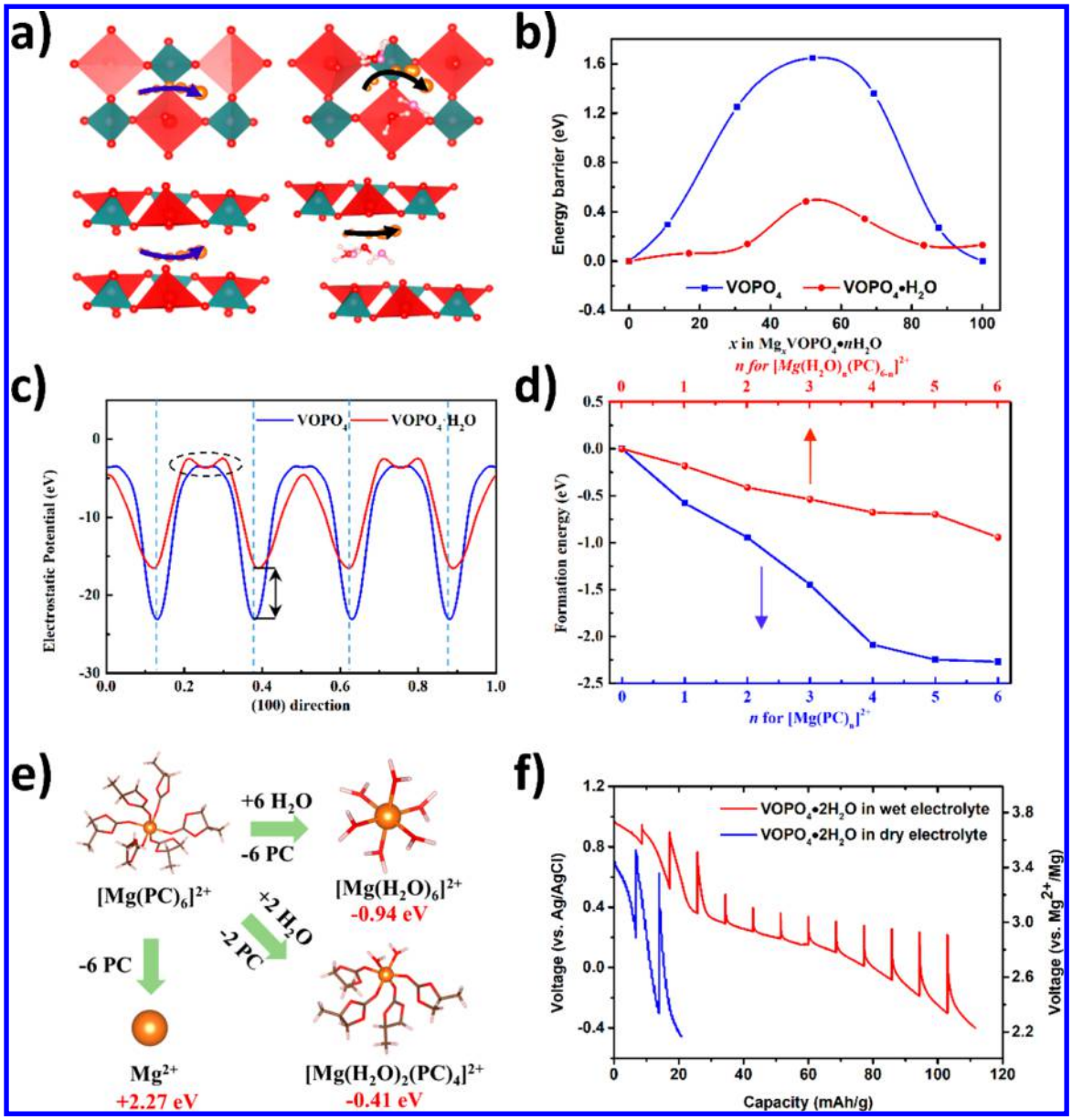

Figure 3. Kinetics of $VOPO_4$ as Mg-ion battery cathode. (a) Illustration of Mg^{2+} diffusion in $VOPO_4$ and $VOPO_4{\cdot}H_2O$ and its corresponding (b) diffusion energy barriers. The red balls represent O atoms of water before diffusion, while the pink balls stand for the O atoms of water after diffusion. (c) Electrostatic potential of $VOPO_4$ and $VOPO_4{\cdot}H_2O$. The black arrow and dashed circle indicate the influence of layer expansion and water dipole effect on electrostatic potential, respectively. (d) Formation energies for $[Mg(PC)_n]^{2+}$ and $[Mg(PC)_n(H_2O)_{6-n}]^{2+}$ ($n \leq 6$). (e) Chemical reaction for $[Mg(PC)_6]^{2+}$ desolvation in different electrolytes. The desolvation energies are also shown next to each complex. (f) GITT profiles for $VOPO_4{\cdot}2H_2O$ in wet and dry electrolytes.

the phase transformation pathway during Mg-ion intercalation, thus changing the reaction kinetics and capacity.

To fully understand the effects of water in $VOPO_4{\cdot}nH_2O$ and in electrolytes on capacity, the reaction kinetics of $VOPO_4{\cdot}nH_2O$ with different H_2O content in dry and wet electrolytes were also investigated. First, the kinetics of Mg^{2+} diffusion in the electrode was assessed. Based on the phase diagram in Figure 2c, the initial states in dry and wet electrolytes are $VOPO_4$ and $VOPO_4{\cdot}H_2O$, respectively. Hence, these two phases were employed to investigate the kinetic characteristics. Figure 3a illustrates the diffusion pathway in $VOPO_4$ and $VOPO_4{\cdot}H_2O$. In $VOPO_4{\cdot}H_2O$ structure, the O atoms of structure water before diffusion are represented by red balls, while the O atoms of structural water after diffusion are represented by pink balls. It is obvious that structural water molecules rotate to accommodate the host structure and Mg^{2+} ions and codiffuse with Mg^{2+} ions. The corresponding energy barriers are plotted in Figure 3b. The diffusion barriers of Mg^{2+} in $VOPO_4$ and $VOPO_4{\cdot}H_2O$ are 1.56 and 0.48 eV, and according to the Arrhenius equation, the room temperature diffusion coefficient of Mg^{2+} ions in $VOPO_4{\cdot}H_2O$ is 1.2×10^{18} times higher than that of $VOPO_4$. The high diffusion barrier in $VOPO_4$ can even block the intercalation of Mg^{2+}. The energy barrier for Mg^{2+} diffusion in $VOPO_4{\cdot}H_2O$ is comparable to that of Mg^{2+} diffusion in spinel metal sulfides and V_2O_5, which are considered to be promising candidates for Mg-ion batteries.[20] The presence of intercalated water significantly lubricates the diffusion of Mg^{2+} ion in the electrode bulk.

DOI: 10.1021/acs.nanolett.8b02854
Nano Lett. 2018, 18, 6441−6448

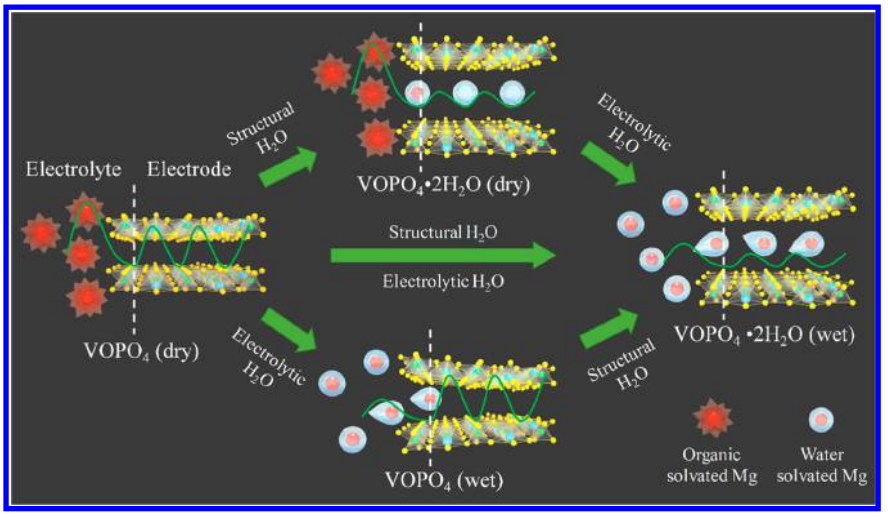

Figure 4. Schematic of charge storage mechanism of $VOPO_4{\cdot}nH_2O$ in dry and wet electrolytes. The green curves indicate the activation energy barriers, and the white dash lines represent the interface of electrolyte and electrode.

The role of water in improving the diffusion process in electrodes was further studied by evaluating the electrostatic potentials along the diffusion path of $VOPO_4$ and $VOPO_4{\cdot}H_2O$ (Figure 3c). The electrostatic potentials show a strong correlation with the energy barriers in Figure 3b. The oscillations of electrostatic potential of $VOPO_4$ are found larger those that of $VOPO_4{\cdot}H_2O$, which indicates a larger change of electrostatic interaction between Mg^{2+} ions and the $VOPO_4$ layer during diffusion. The overview of electrostatic potential difference (black arrow) results mainly from the different interlayer distances. The small local oscillation in the black dashed circle is contributing from the water dipole effect. Therefore, according to the electrostatic potential plot, the electrostatic interaction decrease results mainly from the expanding of the interlayer distance by structural water.

In addition to the diffusion barriers in the electrode, the desolvation energy of Mg^{2+} ions at the interface between electrode and electrolyte is considered to be another main factor for the kinetics because Mg^{2+} ions have to desolvate before intercalation. The formation free energies are calculated to measure the desolvation penalty of Mg^{2+} ions in dry and wet electrolytes. According to the formation energies shown in Figure 3d, the most energetically favorable solvate configuration is $[Mg(PC)_6]^{2+}$ in dry electrolytes. When water exists in the electrolyte, Mg^{2+} ions prefer to solvate with water rather than PC molecules, forming $[Mg(H_2O)_6]^{2+}$ with formation energy of −0.94 eV. During the electrochemical process, the large desolvation energy (2.27 eV) for $[Mg(PC)_6]^{2+}$ makes it difficult for Mg^{2+} ions to desolvate and intercalate (Figure 3e). However, as we mentioned above, water molecules can cointercalate with Mg^{2+} through only partial desolvation (each Mg^{2+} ions solvate six water molecules in liquid electrolyte, but only four water molecules coordinated with Mg^{2+} in the $VOPO_4$ electrode) which apparently makes it easy for Mg^{2+} intercalation.

The reaction kinetics of $VOPO_4{\cdot}2H_2O$ in dry and wet electrolytes at different Mg-ion intercalation levels were also measured using the galvanostatic intermittent titration technique (GITT). As shown in Figure 3f, the overpotential for $VOPO_4{\cdot}2H_2O$ in dry electrolyte is much larger than that in wet electrolyte. As theoretically predicted, the large overpotential of $VOPO_4{\cdot}2H_2O$ in dry electrolytes is attributed to both the large desolvation energy of $[Mg(PC)_6]^{2+}$ and the extremely lower diffusivity of Mg-ion in $VOPO_4$ since the H_2O in $VOPO_4{\cdot}2H_2O$ will transport into dry electrolyte to reach equilibrium.

According to the theoretical analysis, materials characterization, and electrochemical behavior of $VOPO_4{\cdot}nH_2O$ in dry and wet electrolytes, the water activation mechanisms for $VOPO_4$ as Mg-ion battery cathode materials were proposed (Figure 4). During the electrochemical process, the desolvation energy penalty at the interface and diffusion barrier in the electrode act as two gates for Mg^{2+} intercalation. For $VOPO_4$ in dry electrolyte, the Mg-ion intercalation into $VOPO_4$ will first form $Mg_{0.5}VOPO_4$ and then $MgVOPO_4$ with extreme low reaction kinetics due to the very large desolvation energy (2.27 eV) of $[Mg(PC)_6]^{2+}$ and the high diffusion barriers of 1.56 eV of Mg^{2+} in $VOPO_4$. Although $VOPO_4{\cdot}2H_2O$ in wet electrolyte also shows similar two-stage reaction from $Mg_{0.5}VOPO_4{\cdot}2H_2O$ and then $MgVOPO_4{\cdot}2H_2O$, the reaction kinetics is very fast because the water molecules can cointercalate with Mg^{2+} through only partial desolvation, and the diffusion coefficient of $VOPO_4{\cdot}H_2O$ is 1.2×10^{18} times higher than that of $VOPO_4$. As for $VOPO_4$ in wet electrolytes, thermodynamically, the water cointercalates with Mg^{2+} ions, thereby expanding the interlayer distance, stabilizing the $VOPO_4{\cdot}H_2O$ phases, and increasing the equilibrium voltage. However, the presence of water narrows electrolyte decomposition window, limiting the capacity to the value corresponding to one electron per chemical formula. Kinetically, the diffusion barrier in the electrode and desolvation penalty in the interface are largely reduced after water cointerclation into $VOPO_4{\cdot}H_2O$. The presence of structural water in the electrode and electrolytic water in the electrolyte open both of the two gates, releasing the capacity of Mg^{2+} ions. For $VOPO_4{\cdot}2H_2O$ in dry electrolytes, the structural water in the electrode expands the interlayer distance providing the possibility for fast diffusion in the electrode. However, only a small amount of $[Mg(PC)_6]^{2+}$ can desolvate and intercalate into the near-surface. Mg^{2+} ion diffusion into the bulk remains sluggish due to the small interlayer distance. The $VOPO_4{\cdot}2H_2O$ in the wet electrolyte shows decent cycle stability and high Coulombic efficiency (Figure S6, Supporting Information). The stable performance indicates the capacity can be activated and maintained in the

DOI: 10.1021/acs.nanolett.8b02854
Nano Lett. 2018, 18, 6441−6448

layered $VOPO_4$ by the addition of water. Screening additives in electrolyte, which are not only stable with both Mg anode and high voltage layered cathode but also play the similar role as water, can be an effective way to further increase the performance of layered cathode Mg batteries.

In summary, combining electrochemical experiments and DFT calculations, we demonstrate that the capacity of $VOPO_4$ can be largely activated and maintained by introducing water both in $VOPO_4$ structure and in the electrolytes. Water activity in the electrolyte should be larger than 10^{-2} to equilibrate with structural water in $VOPO_4$ to ensure the reversible cointercalation/decointercalation of water-solvated Mg^{2+} ions. The presence of water promotes the voltage but limits the charge transfer of one electron per chemical formula. Water not only lubricates the solid-state diffusion of Mg^{2+} ions in the cathode material but also reduces the penalty of interfacial charge transfer process, releasing the capacity limited by kinetics. The development of novel multivalent-ion batteries should systematically focus on the thermodynamics and kinetics.

■ ASSOCIATED CONTENT

Supporting Information

The Supporting Information is available free of charge on the ACS Publications website at DOI: 10.1021/acs.nanolett.8b02854.

Computational details, experimental details, structure, grand phase diagram, different charge distribution, cyclic voltammetry profiles, and cycle stability (PDF)

■ AUTHOR INFORMATION

Corresponding Authors

*E-mail: cswang@umd.edu.
*E-mail: jiangjj@mail.hust.edu.cn.

ORCID

Ji Chen: 0000-0003-0326-8304
Yunjun Ruan: 0000-0002-0696-8931
Chunsheng Wang: 0000-0002-8626-6381

Author Contributions

X.J. and J.C. synthesized the electrodes, characterized the sample, tested the electrochemical performances, analyzed the results, and wrote the manuscript. F.W. and W.S. synthesized the $VOPO_4$ powder and performed the SEM and TGA tests. X.J., Y.R., L.M., and J.J. designed and conducted the computational works. All authors discussed the results. C.W. supervised the study.

Notes

The authors declare no competing financial interest.

■ ACKNOWLEDGMENTS

The authors acknowledge the insightful discussions with Theodore L. Einstein (University of Maryland, College Park). This work was supported as part of the Nanostructures for Electrical Energy Storage (NEES), an Energy Frontier Research Center funded by the U.S. Department of Energy, Office of Science, Basic Energy Sciences under Award number DESC0001160. We acknowledge the support of the Maryland Nano Center and its AIM Lab. X.J. was supported by a fellowship from China Scholarship Council (201606160018). The authors acknowledge the University of Maryland supercomputing resources (http://hpcc.umd.edu) made available for conducting DFT computations in this paper.

■ REFERENCES

(1) Yang, Z.; Zhang, J.; Kintner-Meyer, M. C.; Lu, X.; Choi, D.; Lemmon, J. P.; Liu, J. *Chem. Rev.* **2011**, *111*, 3577−3613.
(2) Whittingham, M. S. *Chem. Rev.* **2014**, *114*, 11414−11443.
(3) Grey, C.; Tarascon, J. *Nat. Mater.* **2017**, *16*, 45−56.
(4) Thackeray, M. M.; Wolverton, C.; Isaacs, E. D. *Energy Environ. Sci.* **2012**, *5*, 7854−7863.
(5) Lu, J.; Li, L.; Park, J.-B.; Sun, Y.-K.; Wu, F.; Amine, K. *Chem. Rev.* **2014**, *114*, 5611−5640.
(6) Manthiram, A.; Fu, Y.; Chung, S.-H.; Zu, C.; Su, Y.-S. *Chem. Rev.* **2014**, *114*, 11751−11787.
(7) Yabuuchi, N.; Kubota, K.; Dahbi, M.; Komaba, S. *Chem. Rev.* **2014**, *114*, 11636−11682.
(8) Canepa, P.; Sai Gautam, G.; Hannah, D. C.; Malik, R.; Liu, M.; Gallagher, K. G.; Persson, K. A.; Ceder, G. *Chem. Rev.* **2017**, *117*, 4287−4341.
(9) Zhang, R.; Ling, C. *MRS Energy & Sustainability* **2016**, *3*, E1−19.
(10) Aurbach, D.; Lu, Z.; Schechter, A.; Gofer, Y. *Nature* **2000**, *407*, 724−727.
(11) Novák, P.; Shklover, V.; Nesper, R. Z. *Z. Phys. Chem.* **1994**, *185*, 51−68.
(12) Yu, L.; Zhang, X. *J. Colloid Interface Sci.* **2004**, *278*, 160−165.
(13) Lim, S. C.; Lee, J.; Kwak, H. H.; Heo, J. W.; Chae, M. S.; Ahn, D.; Jang, Y. H.; Lee, H.; Hong, S. T. *Inorg. Chem.* **2017**, *56*, 7668−7678.
(14) Nam, K. W.; Kim, S.; Lee, S.; Salama, M.; Shterenberg, I.; Gofer, Y.; Kim, J.-S.; Yang, E.; Park, C. S.; Kim, J.-S. *Nano Lett.* **2015**, *15*, 4071−4079.
(15) Kim, C.; Phillips, P. J.; Key, B.; Yi, T.; Nordlund, D.; Yu, Y. S.; Bayliss, R. D.; Han, S. D.; He, M.; Zhang, Z. *Adv. Mater.* **2015**, *27*, 3377−3384.
(16) Kurihara, H.; Yajima, T.; Suzuki, S. *Chem. Lett.* **2008**, *37*, 376−377.
(17) Sun, X. Q.; Bonnick, P.; Nazar, L. F. *Acs Energy Lett.* **2016**, *1*, 297−301.
(18) Huang, Z.-D.; Masese, T.; Orikasa, Y.; Mori, T. *RSC Adv.* **2015**, *5*, 8598−8603.
(19) Emly, A.; Van der Ven, A. *Inorg. Chem.* **2015**, *54*, 4394−4402.
(20) Liu, M.; Jain, A.; Rong, Z.; Qu, X.; Canepa, P.; Malik, R.; Ceder, G.; Persson, K. A. *Energy Environ. Sci.* **2016**, *9*, 3201−3209.
(21) Wang, R. Y.; Wessells, C. D.; Huggins, R. A.; Cui, Y. *Nano Lett.* **2013**, *13*, 5748−5752.
(22) Chen, L.; Bao, J. L.; Dong, X.; Truhlar, D. G.; Wang, Y.; Wang, C.; Xia, Y. *Acs Energy Lett.* **2017**, *2*, 1115−1121.
(23) Wang, R. C.; Chung, C. C.; Liu, Y.; Jones, J. L.; Augustyn, V. *Langmuir* **2017**, *33*, 9314−9323.
(24) Guduru, R. K.; Icaza, J. C. *Nanomaterials* **2016**, *6*, 41−59.
(25) Yin, J.; Brady, A. B.; Takeuchi, E. S.; Marschilok, A. C.; Takeuchi, K. J. *Chem. Commun.* **2017**, *53*, 3665−3668.
(26) Novák, P.; Imhof, R.; Haas, O. *Electrochim. Acta* **1999**, *45*, 351−367.
(27) Levi, E.; Gofer, Y.; Aurbach, D. *Chem. Mater.* **2009**, *22*, 860−868.
(28) Novak, P.; Desilvestro, J. *J. Electrochem. Soc.* **1993**, *140*, 140−144.
(29) Kim, S.; Nam, K. W.; Lee, S.; Cho, W.; Kim, J. S.; Kim, B. G.; Oshima, Y.; Kim, J. S.; Doo, S. G.; Chang, H. *Angew. Chem., Int. Ed.* **2015**, *54*, 15094−15099.
(30) Doe, R. E.; Downie, C. M.; Fischer, C.; Lane, G. H.; Morgan, D.; Nevin, J.; Ceder, G.; Persson, K. A.; Eaglesham, D. Layered materials with improved magnesium intercalation for rechargeable magnesium ion cells. U.S. Patent 9,401,528, Jul. 26, 2016.
(31) Novák, P.; Scheifele, W.; Joho, F.; Haas, O. *J. Electrochem. Soc.* **1995**, *142*, 2544−2550.
(32) Fuller, T. F.; Newman, J. *J. Electrochem. Soc.* **1993**, *140*, 1218−1225.

DOI: 10.1021/acs.nanolett.8b02854
Nano Lett. 2018, 18, 6441−6448

(33) Sai Gautam, G.; Canepa, P.; Richards, W. D.; Malik, R.; Ceder, G. *Nano Lett.* **2016**, *16*, 2426−2431.
(34) Sa, N.; Kinnibrugh, T. L.; Wang, H.; Sai Gautam, G.; Chapman, K. W.; Vaughey, J. T.; Key, B.; Fister, T. T.; Freeland, J. W.; Proffit, D. L. *Chem. Mater.* **2016**, *28*, 2962−2969.
(35) Wang, F.; Sun, W.; Shadikez, Z.; Hu, E.; Ji, X.; Gao, T.; Yang, X.-Q.; Xu, K.; Wang, C. *Angew. Chem., Int. Ed.* **2018**, *57*, 11978.
(36) Kundu, D.; Adams, B. D.; Duffort, V.; Vajargah, S. H.; Nazar, L. F. *Nat. Energy* **2016**, *1*, 16119−16127.

DOI: 10.1021/acs.nanolett.8b02854
Nano Lett. 2018, 18, 6441−6448